Bulletin of the Seismological Society of America, Vol. 92, No. 6, pp. 2264–2276, August 2002

A New Method for Determining First-Motion Focal Mechanisms

by Jeanne L. Hardebeck and Peter M. Shearer

Abstract We introduce a new method for determining earthquake focal mechanisms from *P*-wave first-motion polarities. Our technique differs from previous methods in that it accounts for possible errors in the assumed earthquake location and seismic-velocity model, as well as in the polarity observations. The set of acceptable focal mechanisms, allowing for the expected errors in polarities and takeoff angles, is found for each event. Multiple trials are performed with different source locations and velocity models, and mechanisms with up to a specified fraction of misfit polarities are included in the set of acceptable mechanisms. The average of the set is returned as the preferred mechanism, and the uncertainty is represented by the distribution of acceptable mechanisms. The solution is considered adequately stable only if the set of acceptable mechanisms is tightly clustered around the preferred mechanism. We validate the method by demonstrating that the well-constrained mechanisms found for clusters of closely spaced events with similar waveforms are indeed very similar. Tests on noisy synthetic data, which mimic the event and station coverage of real data, show that the method accurately recovers the mechanisms and that the uncertainty estimates are reasonable. We also investigate the sensitivity of focal mechanisms to changes in polarities, event depth, and seismic-velocity model, and we find that mechanisms are most sensitive to changes in the vertical velocity gradient.

Introduction

The fault-plane orientations and slip directions of earthquakes can provide important information about fault structure at depth and the stress field in which the earthquakes occur. For large ($M > 4.5$) events, earthquake-source properties can often be found through the inversion of broadband seismic waveforms or geodetic observations. However, the vast majority of earthquakes recorded by local and regional seismic networks are too small to be studied with these techniques. Because of their frequent occurrence, these small earthquakes are particularly important for characterizing regional tectonics and constraining stress orientations.

The source of a small earthquake is typically approximated by a double-couple point source, or focal mechanism, derived from observed *P*-wave first-motion polarities. A focal mechanism divides a reference sphere around the source into four quadrants, two in which the first motion should be away from the source, and two in which it should be toward the source. First-motion polarities are observed at seismic stations, and the position on the focal sphere for each observation, that is, the azimuth and takeoff angle at which the ray leaves the source, is computed for an assumed location and seismic-velocity model. A focal mechanism can then be found that best fits the first-motion observations.

The most widely used method for determining first-motion focal mechanisms from *P*-wave polarity data is the FPFIT software package (Reasenberg and Oppenheimer, 1985). FPFIT employs a grid search over all possible values of the strike, dip, and rake to identify the best-fitting focal mechanism. The misfit for a given focal mechanism is defined as the number of polarity observations that are inconsistent with the predicted polarity for the quadrant in which they appear, weighted by the quality of the observation and the distance from the nodal planes. Confidence intervals for the mechanism strike, dip, and rake are determined by finding how much each parameter may change without exceeding a critical misfit level computed from the observed data misfit.

The FPFIT procedure accounts for the possibility of errors in the observed *P*-wave polarities, but it does not account for possible errors in the computed takeoff angles of the rays. Changes in the assumed source location or the seismic-velocity model alter the pattern of observations on the focal sphere and therefore can change the best-fitting focal-mechanism solution. Mechanisms that are stable with respect to polarity errors may be unstable with respect to small changes in location or velocity model and should not necessarily be considered well constrained.

The representation of uncertainty in terms of a standard error for strike, dip, and rake can also be problematic. Focal mechanisms change nonlinearly in response to changes in

polarities or takeoff angles, so the set of acceptable mechanisms, given the inevitable errors in polarity measurements and computed takeoff angles, is unlikely to form an easily parameterized distribution.

Representing the uncertainty nonparametrically as a set of acceptable mechanisms could be more valuable to users of earthquake catalogs. For example, Lund and Slunga (1999) demonstrate that crustal stress orientations can be more tightly constrained using focal-mechanism catalogs that include a set of acceptable solutions for each event. Focal-mechanism diversity is also an important issue for stress inversion, as well as for seismotectonics. An adequate diversity of mechanisms is necessary for a reliable stress-inversion result (McKenzie, 1969; Hardebeck and Hauksson, 2001), and therefore we would like to be able to distinguish between true mechanism variability and apparent diversity due to errors in polarity measurements and computed takeoff angles. Sets of acceptable mechanisms could be used to test how strongly an apparent diversity of mechanisms is required by the data.

Here we present a new technique for determining first-motion focal mechanisms, which differs from FPFIT primarily in that it accounts for possible errors in earthquake location and seismic-velocity model. We take a nonparametric approach to error estimation, representing the uncertainty as a set of acceptable mechanisms for each event. We test multiple combinations of reasonable locations and velocity structures and compile the set of solutions that fit at least a given fraction of polarity observations. If the set of acceptable mechanisms is tightly clustered, the solution is stable with respect to the expected uncertainty in polarities and takeoff angles and is considered well constrained.

We demonstrate the new focal-mechanism technique by using earthquake data from the region of Northridge, California, between 1981 and 1998, recorded by the Southern California Seismic Network (SCSN). We use earthquake locations obtained using source-specific station terms by Richards-Dinger and Shearer (2000), *P*-wave-polarity data from the SCSN, and corrections for known station polarity reversals (E. Hauksson, personal comm., 2000). The Northridge data are ideal for testing the focal-mechanism technique because they contain ~15,000 located events over a wide range of depths and include a variety of mechanisms (Hauksson *et al.*, 1995). The station coverage is good, as the region is inside the network, and a set of temporary stations was installed after the 1994 *M* 6.7 Northridge mainshock. Although we focus on the Northridge data set to test our method, the principles should apply elsewhere in southern California and to other data sets.

Focal-Mechanism Stability

Before presenting our new method, we will motivate it by demonstrating the sensitivity of first-motion focal mechanisms to various sources of error. The best-fitting focal mechanism depends on the *P*-wave first-motion polarity observations and also the assumed earthquake location and the choice of seismic-velocity model, both of which affect the computed position of rays on the focal sphere. The change in the best-fitting focal mechanism due to changes in polarities and takeoff angles is complex and nonlinear and can depend on other factors, such as station coverage and event depth.

Polarity Errors

Errors in first-motion observations may occur because of station polarity reversals or incorrect direct *P*-arrival picks due to low signal-to-noise ratios. First-motion observations are usually divided by analysts into two classes: impulsive, for which polarities are easily determined; and emergent, for which the polarities are more ambiguous. Impulsive-polarity observations are of higher quality but still may contain errors.

The stability of a focal mechanism with respect to polarity errors can be tested by changing a single polarity datum and observing the change in the best-fitting mechanism. The focal mechanism in Figure 1 is apparently well constrained, in that the best-fitting solutions fit all of the impulsive-polarity observations and are tightly clustered. When one polarity observation is reversed, however, the best-fitting mechanisms are of a completely different faulting style, indicating that the solution is highly unstable with respect to the polarity observations.

The actual rate of polarity errors will vary between data sets. For the 1981–1998 Northridge SCSN catalog, we estimate the polarity-error rate by using clusters of similar earthquakes identified from waveform cross correlation. The similar waveforms imply that the mechanisms of the events are very similar and that the observed polarity at a given

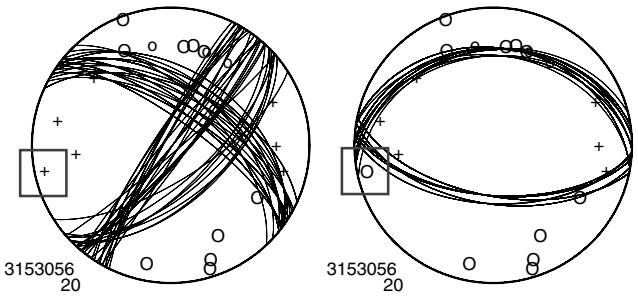

Figure 1. An example of a focal mechanism that appears to be well constrained but is unstable with respect to first-motion polarity errors. (Left) *P*-wave polarities (+, impulsive up; *x*, emergent up; O, impulsive down; o, emergent down) and the set of focal mechanisms that fit all of the impulsive polarities. (Right) The set of best-fitting focal mechanisms when the highlighted polarity is reversed. The top number under each mechanism is the SCSN-assigned identification number of the event, the bottom is the number of polarity observations. The takeoff angles were computed using the 1D velocity-model SOCAL (Fig. 5).

station should be the same for each event in a cluster. For similar event clusters in the Northridge region (Shearer *et al.*, 2002), we find that ~10% of the impulsive polarities and ~20% of the emergent polarities are inconsistent, after correcting for known station polarity reversals. We take this to be the approximate polarity error rate for the SCSN data.

Event Location

Changes in event location can alter the computed position of rays on the focal sphere and therefore, the best-fitting focal mechanism. We will focus on the sensitivity of focal mechanisms to changes in event depth, because vertical uncertainty is usually much larger than horizontal uncertainty. For a 1D seismic-velocity model, depth errors will affect only the computed takeoff angle, as the computed azimuth at which the ray leaves the source will always be the source-to-station azimuth. Unless the horizontal velocity contrasts are extremely large, the computed azimuth for a 3D velocity model will also be well approximated by the source-to-station azimuth. For example, for the southern California 3D velocity model of Hauksson (2000), ~99% of the computed ray azimuths are within 1° of the source-to-station azimuth (Fig. 2).

To demonstrate the change in takeoff angle due to a change in source depth, we consider takeoff angles computed from the 1D seismic-velocity model SOCAL, a smoothed version of a standard, southern California velocity model (Shearer, 1997). We test a range of initial source depths and takeoff angles and determine the change in takeoff angle for a 1-km change in depth (Fig. 3). A vertical uncertainty of ~1 km is typical of regional earthquake locations. Significant changes in takeoff angle (≥5°) are observed for events shallower than ~7 km, with the largest changes, up to ~15°, for events near the surface.

The change in takeoff angle for upgoing rays (takeoff angle <90°) is generally greater than for near-horizontal rays (takeoff angle ≈90°) or downgoing rays (takeoff angle >90°). A typical earthquake recorded by the SCSN has many more near-horizontal and downgoing rays than upgoing rays, so the majority of takeoff angles should be relatively stable. However, individual upgoing rays can be very important in constraining a focal mechanism, because this portion of the focal sphere is usually sparsely sampled, so instability of these takeoff angles may lead to mechanism instability.

A summary of the change in best-fitting focal mechanism caused by a ±1-km change in source depth for ~1500 Northridge events is shown in Figure 4. In general, the angular change is not large, <20° for 81% of the events. (The angular difference between two mechanisms is defined as the minimum rotation, about any axis, needed to make the two identical.) Earthquakes shallower than ~10 km are the most sensitive to changes in depth. Strike-slip events appear to be slightly less sensitive than dip-slip events. This is expected, because for a pure strike-slip event, the takeoff angle can be changed, and the observation will always stay in the

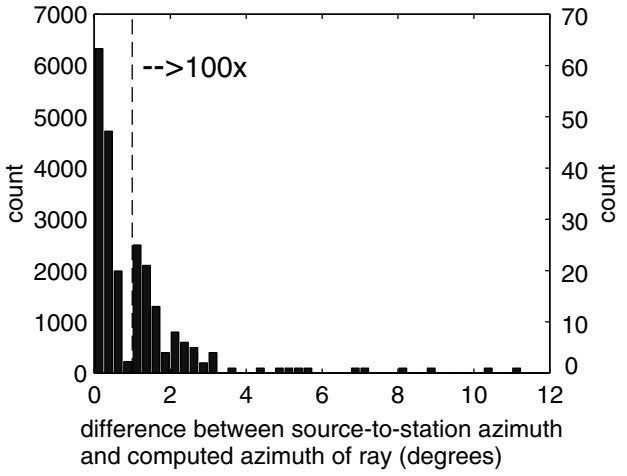

Figure 2. The difference between the azimuth at which a ray leaves an earthquake source, computed using the southern California 3D seismic-velocity model of Hauksson (2000), and the source-to-station azimuth. The ray azimuths were computed by E. Hauksson (personal comm., 2000) for data from ~300 Northridge aftershocks. The histogram to the right of the dashed line at 1° is exaggerated 100 times relative to the histogram to the left of the line.

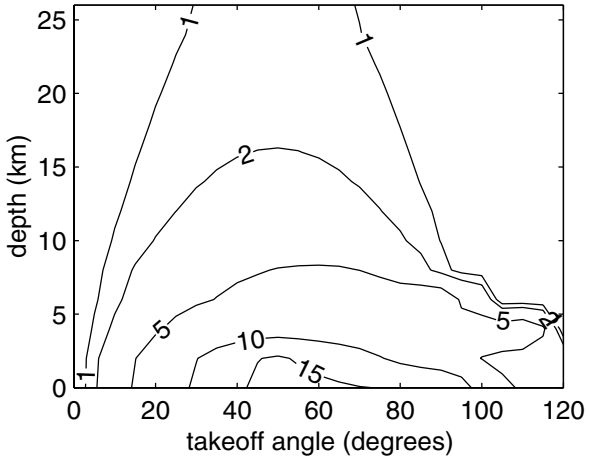

Figure 3. The contours show the change in ray takeoff angle due to a ±1-km change in depth for a range of original source depths and takeoff angles. Takeoff angle is measured down from upward vertical and was computed using the 1D seismic-velocity model SOCAL (Fig. 5). Takeoff angles between 0° and 90° represent rays that travel upward from the source; rays at takeoff angles >90° leave the source in a downward direction. The relationship between takeoff angle and range was found by tracing the paths of 9000 rays spanning reasonable values of the ray parameter through a 1D gradient-velocity model.

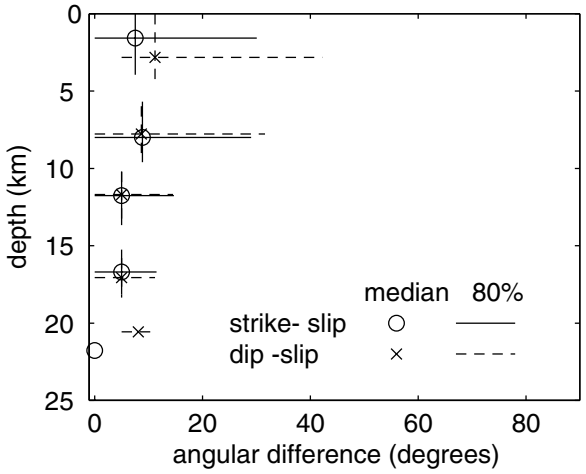

Figure 4. The angular difference in focal mechanism caused by a ± 1-km change in source depth for ~1500 Northridge earthquakes. The best-fitting mechanisms were found using FPFIT. For each event, the mechanisms for both the original and perturbed source depth were well constrained (1σ uncertainty in strike, dip, and rake of $\leq 25°$; a misfit of ≤ 0.15; and an STDR ≥ 0.5.) The angular difference is defined as the minimum rotation, about any axis, required to align the two mechanisms. If FPFIT found multiple solutions, the difference between the closest two is used. Strike-slip events are defined as those having a rake direction $\leq 35°$ from horizontal; all others are dip slip. The mean angular difference and the middle 80% for 5-km depth intervals are shown.

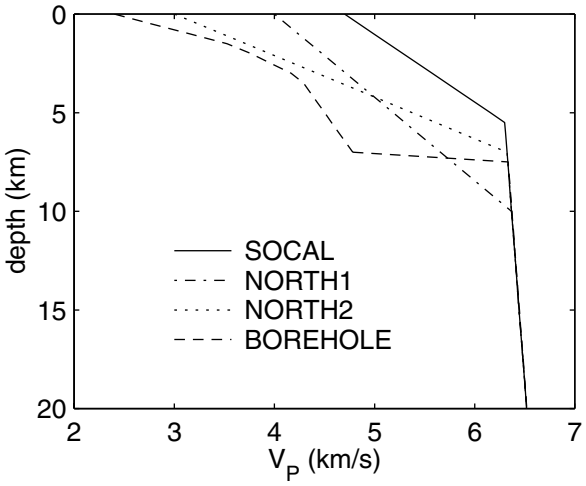

Figure 5. Four sample 1D velocity models for the Northridge region: SOCAL, a smoothed version of a standard model for southern California (Shearer, 1997); NORTH1 and NORTH2, two models that include low seismic velocities at shallow depths to model the basin structure of the San Fernando Valley; and BOREHOLE, a model inferred from seismic-velocity profiles in boreholes (J. Shaw, personal communication, 2000), which features a sharp velocity gradient at the sediment–bedrock interface.

same quadrant of the focal mechanism. In the dip-slip case, however, changing the takeoff angle may move the observation between mechanism quadrants.

Seismic-Velocity Model

The computed distribution of observations on the focal sphere and therefore, the best-fitting focal mechanism, is also dependent on the choice of seismic-velocity model. As with event location, the major effect is on the computed takeoff angle. For 1D velocity models, the computed azimuth is always the source-to-station azimuth. For a 3D velocity model, even one containing significant horizontal velocity differences owing to complex crustal structure, these two azimuths will still be approximately the same (Fig. 2).

The sensitivity of the takeoff angle to the velocity model is usually much greater than the sensitivity to event depth. We explore four different 1D seismic-velocity models that span a range of possible structures for the Northridge region (Fig. 5): the general southern California model SOCAL as described previously; NORTH1 and NORTH2, which include low seismic velocities at shallow depths to model the basin structure of the San Fernando Valley; and the model BOREHOLE, based on seismic-velocity profiles in boreholes (J. Shaw, personal communication, 2000), which also includes low seismic velocities at shallow depths, with a sharp velocity gradient at the sediment–bedrock interface. A comparison of takeoff angles computed from these models is shown in Figure 6. The discrepancy between the takeoff angles computed from the different models is often 20°–40°. Only for source depths of at least 10 km, the depth below which all of the models are the same, are all of the computed takeoff angles within ~10° of each other.

The computed takeoff angle is most dependent on the vertical gradient of the seismic velocity, as the gradient controls the depth at which the ray turns. The magnitude of the seismic velocity is less important; for instance, if a velocity model were scaled by a constant, the computed ray paths would be unchanged. Above 5 km, where the models SOCAL and NORTH1 have similar velocity gradients, although different average velocities, the takeoff angles for upgoing rays are nearly identical. In contrast, the models NORTH1 and NORTH2, which have similar average velocity in the upper 10 km but different gradients, have dissimilar takeoff angles for events in this depth range. Also apparent at shallow source depths is a steep change in takeoff angle at a critical source-to-station distance for the model BOREHOLE, because of its sharp velocity gradient at ~7-km depth.

Focal mechanisms are also more sensitive to a change in seismic-velocity model than to a change in source depth. Mechanisms for ~1700 Northridge events were computed using the four example velocity models. For each event, four mechanisms were found, one using each velocity model. We compare all the possible pairs of well-constrained solutions for each event. Figure 7 shows a summary of the angular difference between each pair of solutions. Events deeper

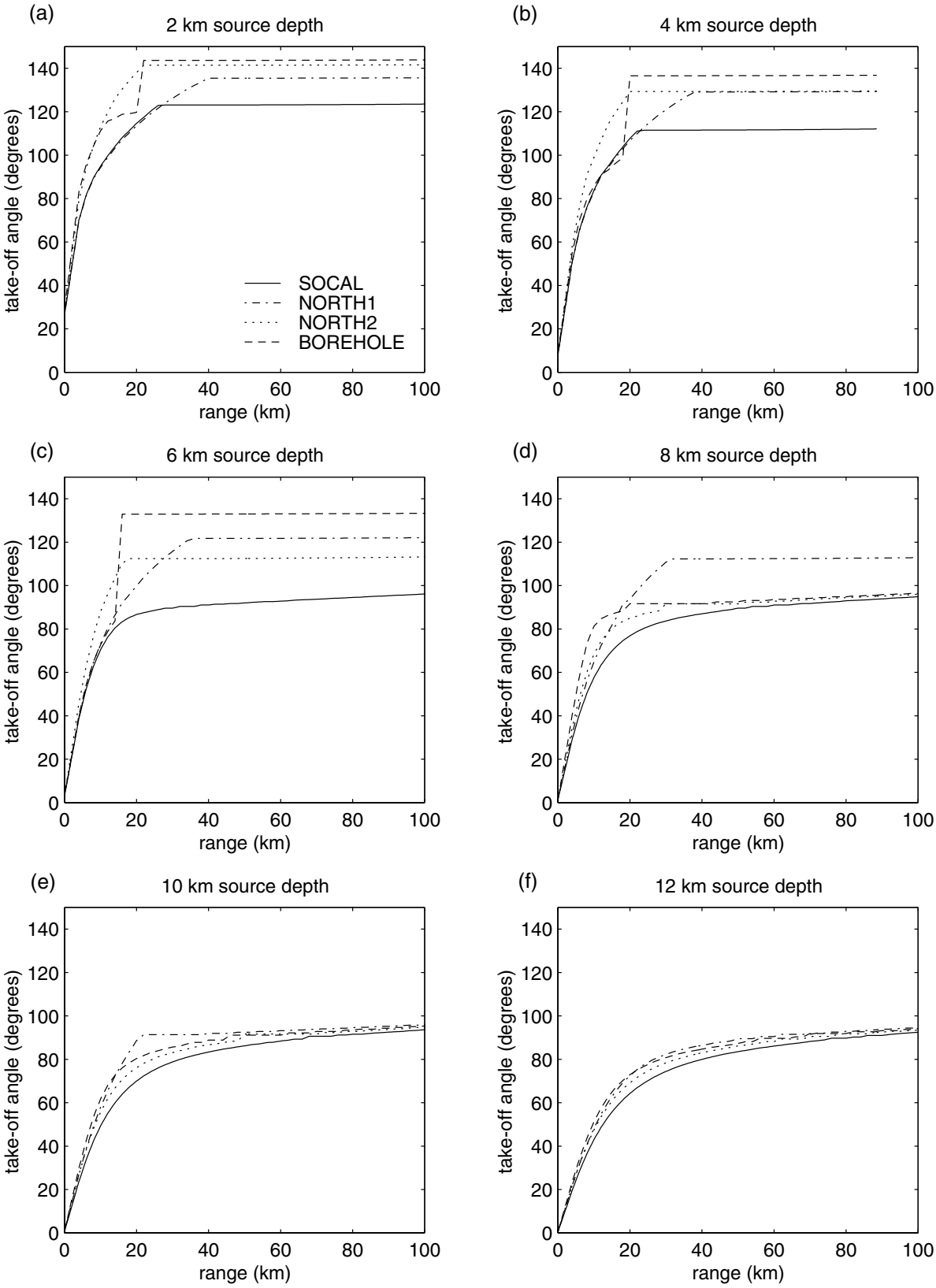

Figure 6. The computed takeoff angle versus range (the distance from the epicenter to the station) for the four 1D seismic velocity models shown in Figure 5, for six different source depths: (a) 2 km; (b) 4 km; (c) 6 km; (d) 8 km; (e) 10 km; (f) 12 km. Takeoff angle is measured down from upward vertical.

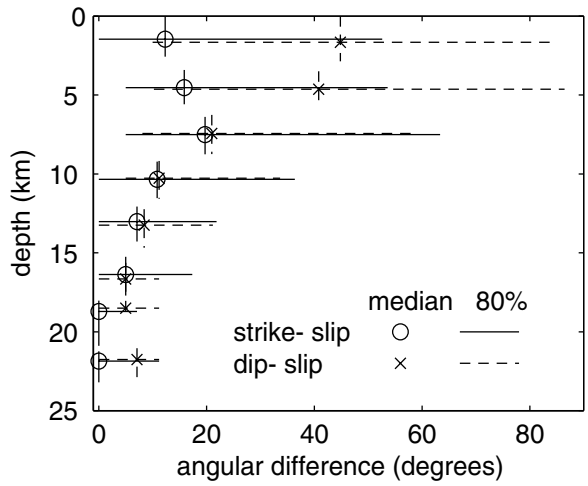

Figure 7. The angular difference between focal mechanisms computed using the different 1D velocity models shown in Figure 5. Focal mechanisms were found using FPFIT for each velocity model for ~1700 Northridge earthquakes. Four mechanisms were found for each event, one for each velocity model, and all pairs of well-constrained solutions (1σ uncertainty $\leq 25°$, misfit ≤ 0.15, and STDR ≥ 0.5) are included. Strike-slip events are those with a rake direction $\leq 35°$ from horizontal; others are dip slip. The mean angular difference and the middle 80% for 3-km depth intervals are shown.

than 10 km are the most stable, with 83% of mechanism pairs within 20° of each other and 90% within 30°. Deep strike-slip events are only slightly more stable than deep dip-slip events. Strike-slip events above 10 km depth are more sensitive to velocity model changes than the deeper events, with 60% of mechanism pairs within 20° of each other and 74% within 30°. Shallow dip-slip events are the most unstable with respect to velocity model, with only 61% of mechanism pairs within 30° of each other. The shallow events tend to be more unstable in this example because the variation in the velocity models is limited to the upper 10 km.

Method

We introduce a new technique for determining first-motion focal mechanisms, in light of the sensitivity of the best-fitting mechanisms to errors in polarity observations and computed takeoff angles. The central idea is to find the set of all mechanisms for each event that are acceptable, given the expected polarity error rate and the range of allowed source locations and seismic-velocity models. If this set is tightly clustered, this indicates that the solution is stable with respect to errors and can be considered well constrained. The method is outlined in Figure 8.

For an initial event location and seismic-velocity model, we compute takeoff angles and perform a grid search over strike, dip, and rake to find the set of acceptable focal mechanisms. We first identify the mechanisms that minimize the number of misfit impulsive polarities. If there are multiple mechanisms that fit all of the impulsive polarities, the subset that also minimizes the number of misfit emergent polarities is chosen. (No additional weighting of the data is done. FPFIT down-weights near-nodal data because of potential errors in these polarities. However, this can sometimes result in the selection of mechanisms for which the majority of observations lie along the nodal planes, as this artificially reduces the misfit.) Because of the possibility of polarity errors, mechanisms with additional misfit polarities are also included in the set of acceptable mechanisms. For the SCSN data, we allow mechanisms with up to 10% misfit impulsive polarities, or the minimum misfit plus 5% if this is greater.

Multiple trials are performed using takeoff angles computed from different combinations of possible source depths and seismic-velocity models, and the acceptable mechanisms found for each trial are added to the cumulative set of acceptable solutions for the event. The number of trials is limited by computational speed and trades off with grid spacing. We usually perform 50 trials with a 5° grid. The event depth is chosen randomly from a normal distribution based on the vertical standard error reported by the earthquake-location method. The velocity model is chosen from a set of models that span a reasonable range of velocity structures. For the Northridge events, we use SOCAL and four local 1D averages of 3D velocity models (Fig. 9). For the examples in this article, we make the simplifying assumption that the depth and velocity-model errors are uncorrelated, but the method also can be used with correlated errors.

The preferred solution is that which is most probable, given the distribution of acceptable mechanisms. If the majority of the acceptable mechanisms are clustered, the correct solution is mostly likely to fall within that cluster. The preferred solution is therefore found by averaging the acceptable solutions, after removing any outliers. (The average solution is found by averaging the normals to the nodal planes in vector coordinates.) We iteratively remove the mechanism farthest from the average, and then compute a new average until all of the remaining mechanisms are within 30° of the average. This ensures that if there are multiple clusters of solutions, the preferred mechanism is approximately the average of the more probable cluster, not a weighted average of all of the clusters. The fraction of acceptable solutions that are within 30° of the preferred solution gives an estimate of how likely it is that the correct solution is within the chosen cluster.

The confidence regions are expressed nonparametrically as the set of acceptable mechanisms for each earthquake. If the set of acceptable mechanisms is tightly clustered around the preferred mechanism, the solution is stable with respect to possible errors. The spread of the solutions is measured by the root-mean-square (RMS) angular difference between the acceptable mechanisms and the preferred mechanism. The RMS rotation angle can be used as the 1σ mechanism uncertainty when a concise representation is necessary.

We rate the quality of a mechanism based on the tight-

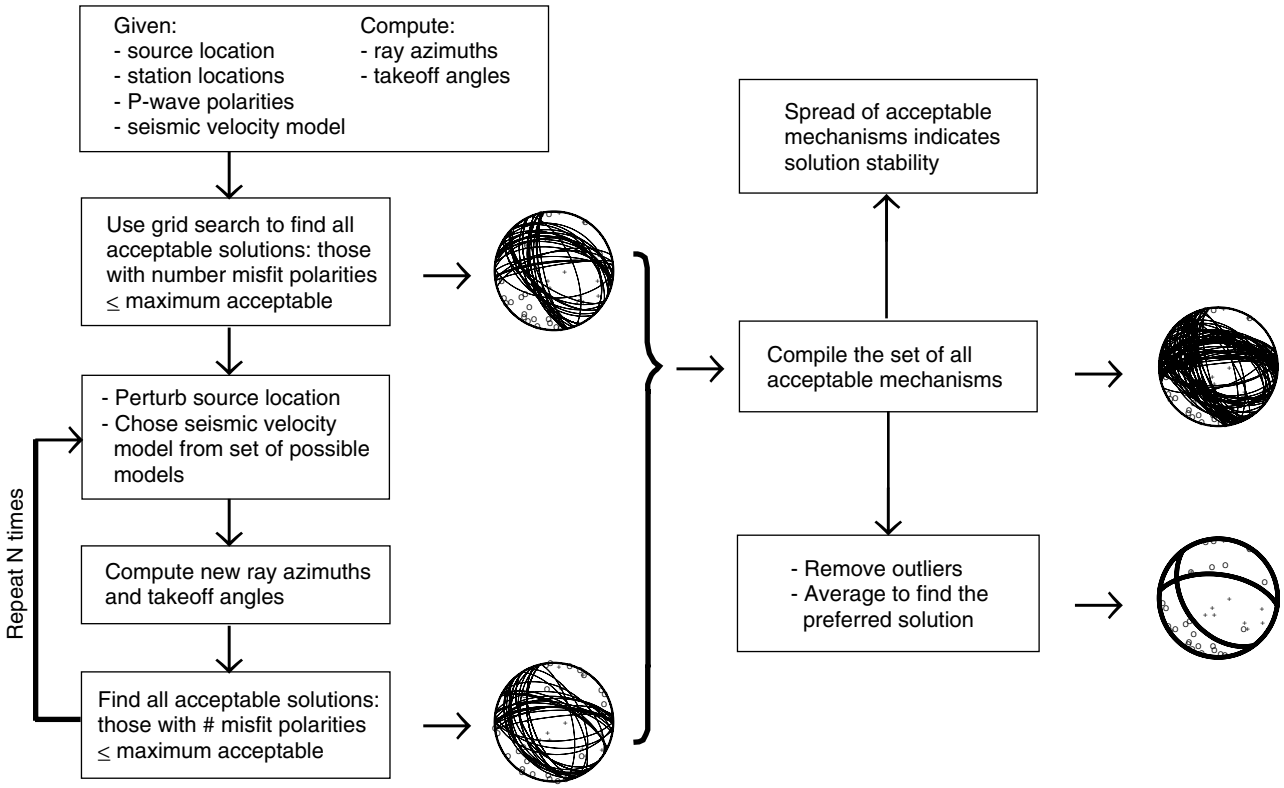

Figure 8. A flowchart of the new method for determining earthquake focal mechanisms described in the text.

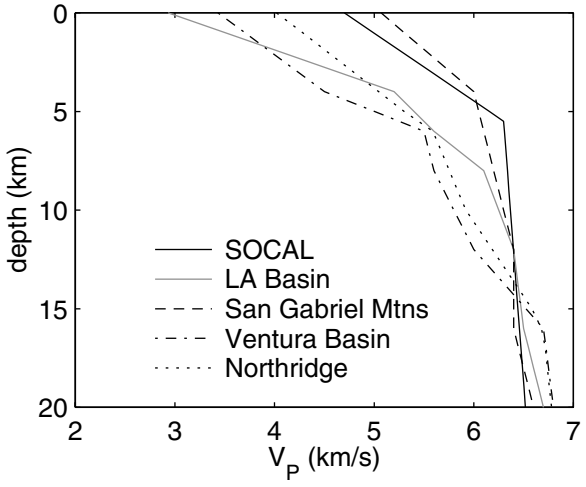

Figure 9. The 1D velocity models for the Northridge region used to compute focal mechanisms: SOCAL, as in Figure 5; LA Basin, San Gabriel Mtns, and Ventura Basin, average models for these regions from Hauksson and Haase [1997]; and Northridge, an average of the 3D velocity model of Hauksson [2000] in the vicinity of Northridge.

ness of the set of acceptable mechanisms and the number of misfit polarities for the preferred solution. Two measures of tightness are used: the RMS difference from the preferred solution and the fraction of the acceptable solutions that are within 30° of the preferred solution. The reported polarity misfit for the prefered solution is computed similarly to FPFIT, with down-weighting of the near-nodal data, so that results from the two methods can easily be compared (this down-weighting is done only for this comparison and has no effect on our solutions). We also compute the station distribution ratio (STDR), introduced by Reasenberg and Oppenheimer (1985). The STDR quantifies how the observations are spaced on the focal sphere, relative to the nodal planes, with a larger STDR indicating a better distribution. The STDR has been shown to be a good indicator of mechanism quality (Kilb, 2001).

For the examples in this article, quality A requires an RMS difference of $\leq 25°$, $\geq 90\%$ of the mechanisms within 30° of the preferred mechanism, a misfit of $\leq 15\%$ of the polarities, and STDR ≥ 0.5; quality B, RMS difference $\leq 35°$, $\geq 60\%$ within 30°, misfit $\leq 20\%$, and STDR ≥ 0.4; quality C, RMS difference $\leq 45°$, $\geq 50\%$ within 30°, misfit $\leq 30\%$, and STDR ≥ 0.3; and all others are quality D.

Focal mechanisms can be reliably determined only for events with first-motion observations that adequately sample the focal sphere. The examples shown in this article include

only events with at least eight polarity observations. The maximum gap in the source-to-station azimuth is required to be $<90°$, and the maximum gap in takeoff angle is required to be $<60°$ (i.e., the takeoff angles cannot be all near-horizontal or all near-vertical).

Validation

Validating a method for determining focal mechanisms can be difficult because the true focal mechanisms, event locations, and seismic-velocity structure are not known. One approach is to create synthetic data sets for which the correct mechanisms are known. An alternative is to compare the focal mechanisms of clusters of closely spaced earthquakes with similar waveforms. The similar events should have similar focal mechanisms, so for these earthquakes, we do in a sense know the correct focal mechanism. We perform several different tests, with both real and synthetic data, to demonstrate that the solutions obtained by our technique are reasonable and are an improvement over those obtained by FPFIT.

Real Data

Not surprisingly, the well-constrained mechanisms found by our method are often similar to the well-constrained mechanisms obtained by FPFIT, given the same station distributions and polarity observations. For 222 Northridge events, quality A or equivalent focal mechanisms were found by using both techniques. The angular differences between the two mechanisms for each event are shown in the histogram in Figure 10. For ~90% of the events, the two are within 25° of each other. Given that the average 1σ uncertainty of the quality A mechanisms is ~20°, the discrepancies are generally not significant.

Some of the Northridge events occur in spatial clusters with very similar waveforms (Shearer *et al.*, 2002), implying that the earthquakes have approximately the same source. Quality A solutions for the largest cluster of similar events are shown in Figure 11. The focal mechanisms are indeed very similar, which we interpret to mean that they are accurate. Most are somewhat oblique thrust mechanisms with NNE-trending compressional axes. Three events have slightly different mechanisms: events 3142984 and 3150301, which are nearly pure thrust, and event 3153955, which is oblique in the opposite sense from the others. However, all of the sets of acceptable solutions overlap. The sets of acceptable solutions for the more poorly constrained events also all include solutions similar to the A-quality mechanisms, indicating that the data do not require significant mechanism diversity within the cluster.

We also use FPFIT to find mechanisms for the same cluster of similar events. For many events, the mechanisms found by the two techniques are in close agreement. However, the set of mechanisms found by FPFIT also includes four apparently good-quality mechanisms that are dissimilar from the rest of the solutions (Fig. 12). For two of these events (3141745 and 3143016), FPFIT finds a thrust mechanism with a NNE-trending compression axis, but our prefered solution is closer to the mechanisms in Figure 11. For the other two (3143730 and 3154048), the FPFIT solution has an ESE-trending compression axis. The set of acceptable mechanisms for these events are quite diverse, indicating that the solutions are unstable with respect to uncertainty in the observed polarities and computed takeoff angles. Our preferred solutions are again more similar to those in Figure 11, and lower-quality ratings are given.

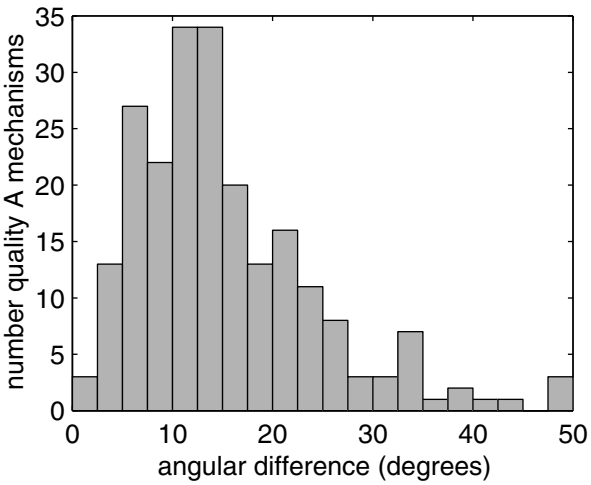

Figure 10. A histogram of the angular difference between focal mechanisms determined by the technique introduced in this article and those determined by FPFIT for 222 Northridge earthquakes with quality A solutions. The FPFIT solutions are all quality A equivalent, with a 1σ uncertainty in strike, dip, and rake of $\leq 25°$, misfit ≤ 0.15 and STDR ≥ 0.5. The same polarity data were used by both techniques. The takeoff angles used by FPFIT were found from the model SOCAL (Fig. 5). Our method uses the five 1D velocity models shown in Figure 9. If FPFIT found multiple solutions, the difference from the closest solution is used.

Our method better captures the similarity of the mechanisms for this cluster. For the four examples in Figure 12, the preferred mechanisms selected by our technique match the inferred correct solution more closely than the best-fitting mechanisms found by FPFIT. In these cases, it appears that the FPFIT algorithm has found a solution which "threads the needle" between the different polarities, obtaining a mechanism that has low misfit for one particular assumed event location and seismic-velocity model. In contrast, our approach of finding the most probable solution, given a range of possible locations and velocity models, appears more successful in identifying the correct mechanism.

Synthetic Data

Another way to test our focal-mechanism technique is with realistic synthetic data. We can evaluate how well our technique recovers the correct solutions because they are

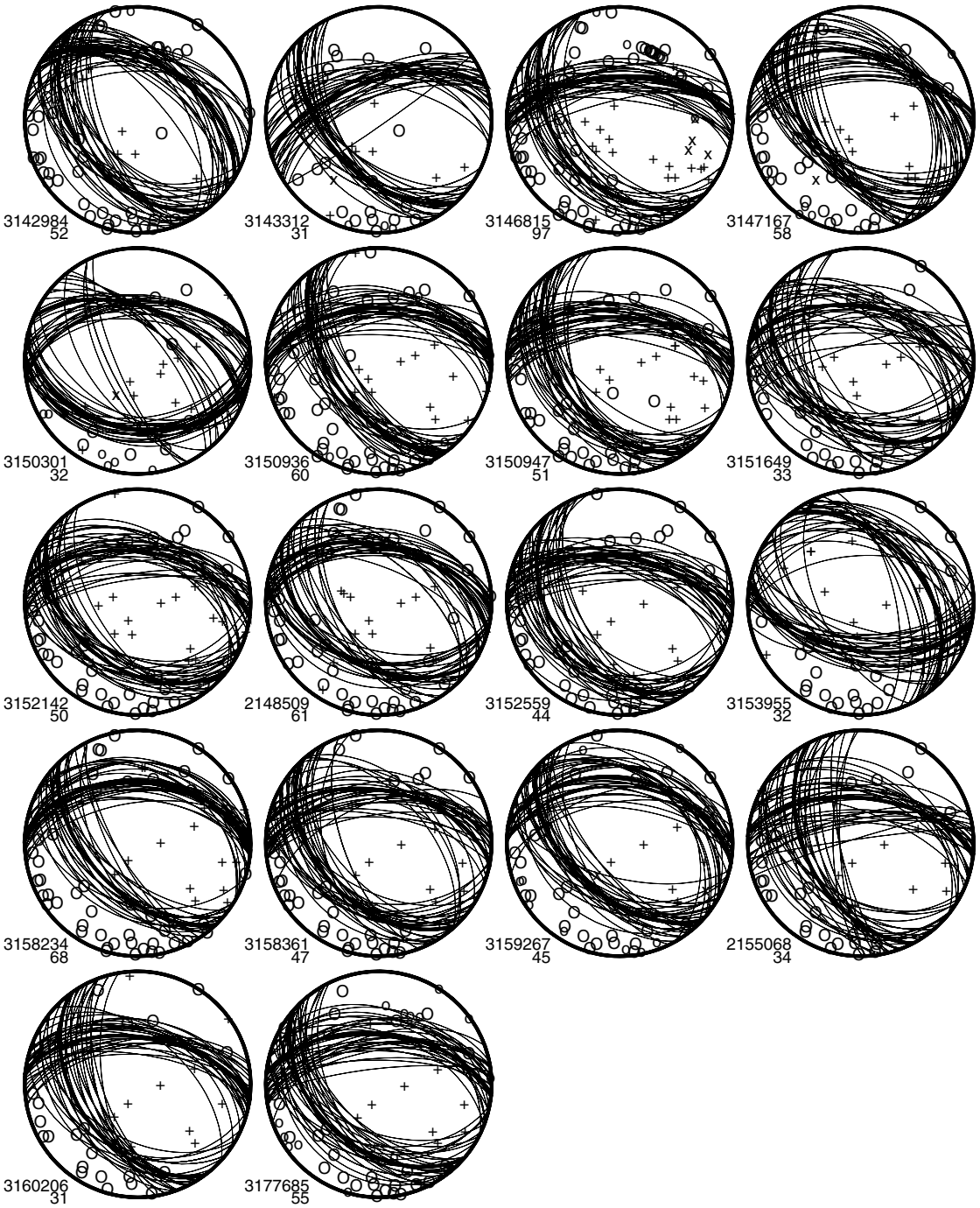

Figure 11. Quality A focal mechanisms for a cluster of similar events in the Northridge aftershock sequence, identified using waveform cross correlation (Shearer *et al.*, 2002). The thick lines indicate the preferred mechanisms, whereas the thin lines show 50 mechanisms chosen from the set of acceptable mechanisms. Takeoff angles shown were computed using the SOCAL velocity model (Fig. 5). Polarity symbols are as in Figure 1.

known. Additionally, if many synthetic tests are performed, we can also test the appropriateness of the confidence regions.

We generate a set of synthetic earthquakes for Northridge by selecting focal mechanisms with random orientations. The station distribution for a randomly selected real Northridge event is used, and the polarity at each station is assigned to be consistent with the chosen focal mechanism and source depth, assuming the 3D velocity model of Hauksson (2000). We use the set of source and station locations and polarities as input into our focal-mechanism method. Realistic errors in polarity, source depth, and velocity model

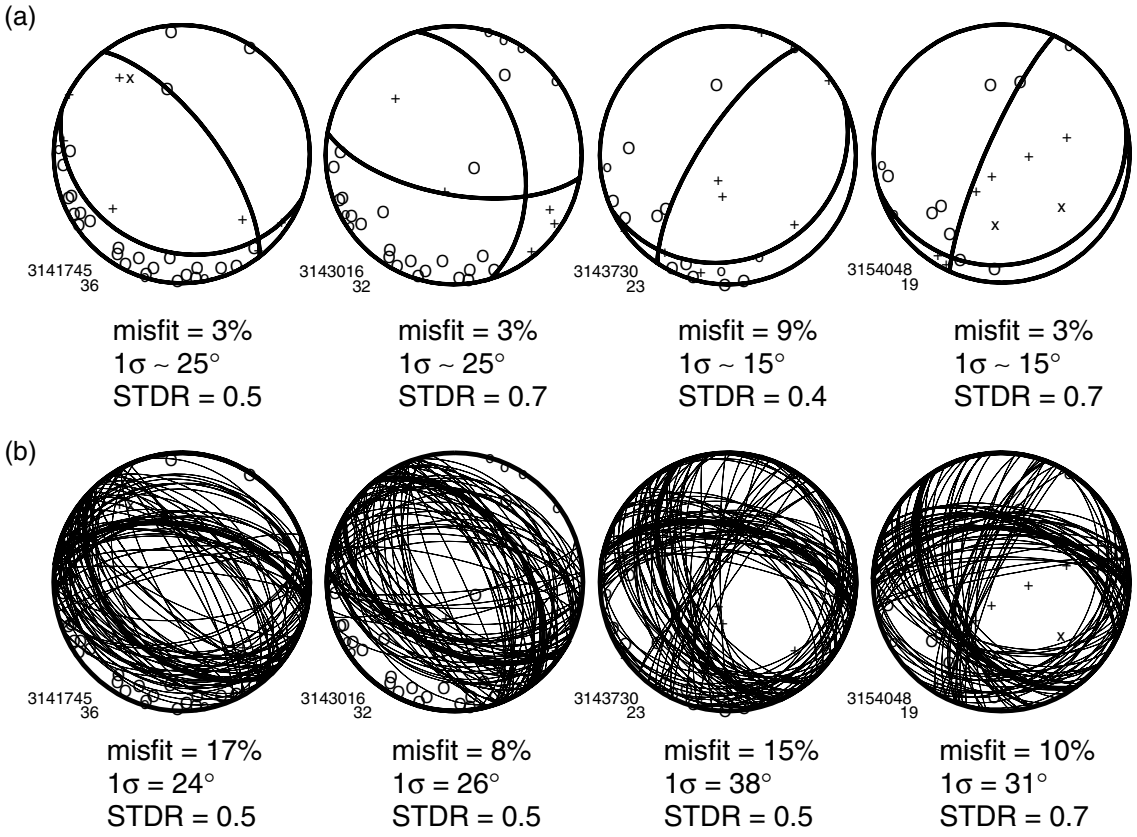

Figure 12. A comparison of focal mechanisms found by FPFIT and our method for four earthquakes in the same similar event cluster as the earthquakes in Figure 11. (a) FPFIT best-fitting solutions, with misfit, uncertainty, and STDR. All qualify as quality A equivalent, except for event 3143730 with STDR < 0.5, which still might be considered acceptable after visual inspection of the station distribution. Event 3154048 has two solutions, but the other one did not converge, so it was discarded. (b) Our solutions, with misfit, uncertainty, and STDR. All are quality B or lower. The thick lines indicate the preferred mechanisms, whereas the thin lines show 50 mechanisms chosen from the set of acceptable solutions. Takeoff angles shown were computed using the SOCAL velocity model (Fig. 5). Polarity symbols are as in Figure 1.

are included. Polarity errors are introduced with a 10% probability, and random depth perturbations with a standard error of 1 km are added. We use the 1D models shown in Figure 9 to determine the focal mechanisms, simulating the common situation of approximating actual 3D structure with 1D models.

The method is generally successful in recovering the correct focal mechanisms, especially for the well-constrained solutions (Fig. 13). For the A- and B-quality mechanisms, which make up ~40% of the data set, ~60% of the computed preferred mechanisms are within 20° of the correct mechanism, and ~80% are within 30°. For quality A, the mean angular difference between the computed preferred and correct mechanisms is ~18°; quality B, ~22°; quality C, ~23°; and quality D, ~28°.

We then test the appropriateness of the uncertainty estimates. If they are a good approximation of the true error, the correct solution should fall inside the 95% confidence region for approximately 95% of the events. The RMS angular difference between the acceptable mechanisms and the preferred mechanism appears to be a good approximation of the 1σ mechanism uncertainty, as the angular misfit between the correct and preferred mechanisms is $<2\sigma$ for ~95% of the events (Fig. 14). Ideally, the correct mechanism will always appear in the set of acceptable solutions. For most ranges of source parameters, the correct solution falls within the set of acceptable mechanisms for ~99% of the events (Fig. 14). The only exception is for ~15–20-km-source depths, where it is within the set for ~95% of events, probably because the 1D seismic-velocity models are very similar at depth and do not adequately span the range of velocity structures present in the 3D model.

Discussion

Although the *P*-wave first-motion focal mechanisms found using the FPFIT technique have been valuable in numerous seismotectonic studies, there are ways in which the

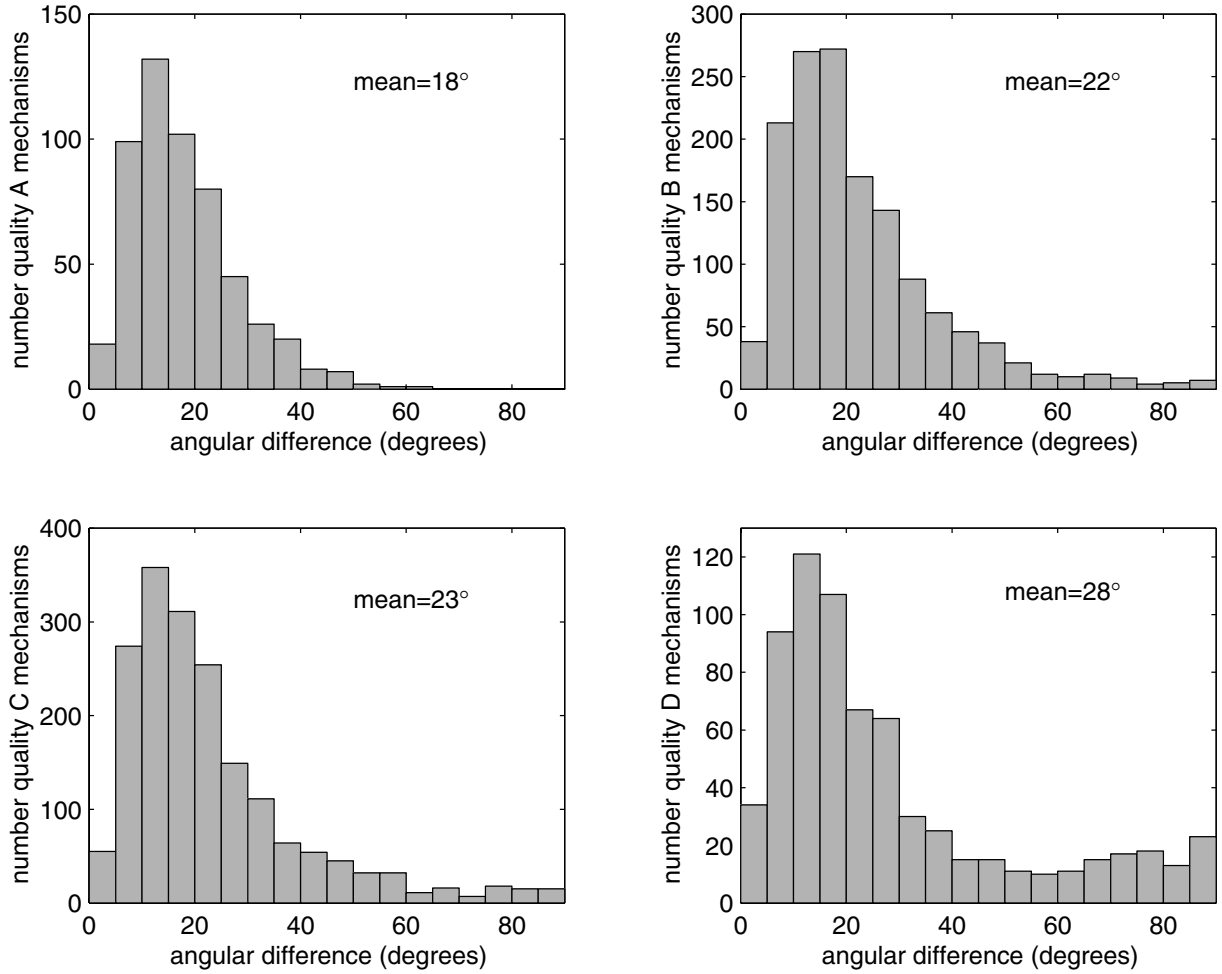

Figure 13. Histograms of the angular difference between the correct and computed mechanisms for tests with synthetic data. The synthetic mechanisms were designed assuming the 3D velocity model of Hauksson (2000) and the computed mechanisms obtained with our algorithm and the suite of 1D velocity models shown in Figure 9. Five thousand synthetic events were created with random focal mechanisms, and the *P*-wave polarities were assigned using the station distributions of real Northridge events. Realistic errors were simulated by randomly reversing the polarities of 10% of the measurements, changing the source depth randomly with $1\sigma = 1$ km, and using the 1D velocity models, which only approximate the assumed velocity structure.

computation of focal mechanisms for small earthquakes can be improved. One strategy is to increase the quality and quantity of the data and incorporate additional sources of information. This is an important approach, because in some cases, (e.g., where the existing station distribution is inadequate), this may be the only way to achieve significant improvements in focal-mechanism accuracy. However, if the input data are limited to existing *P*-polarity measurements, improvements are still possible if the methodology can be made more reliable. Our new technique does so by contributing solutions to several potential problems.

One difficulty is that focal mechanisms are highly sensitive to changes in source location and seismic-velocity model. The mechanisms are most sensitive to the vertical velocity gradient, because the gradient controls the turning depth of the rays and hence, the relationship between range and takeoff angle. It is sobering to find that takeoff angles and focal mechanisms are very sensitive to the vertical gradient of the velocity model. While the general crustal velocity structure can be found from travel-time inversions, the details of the vertical gradient are usually poorly constrained. We present a technique for accounting for the expected errors by finding mechanisms for a suite of possible locations and velocity models. Because of the complexity and nonlinearity of the dependence of takeoff angle on location and velocity model, it seems unlikely that the sensitivity could be studied in a more elegant or general way.

Another problem is that the complex sensitivity of focal mechanisms to changes in polarity observations and computed takeoff angles makes the range of reasonable solutions

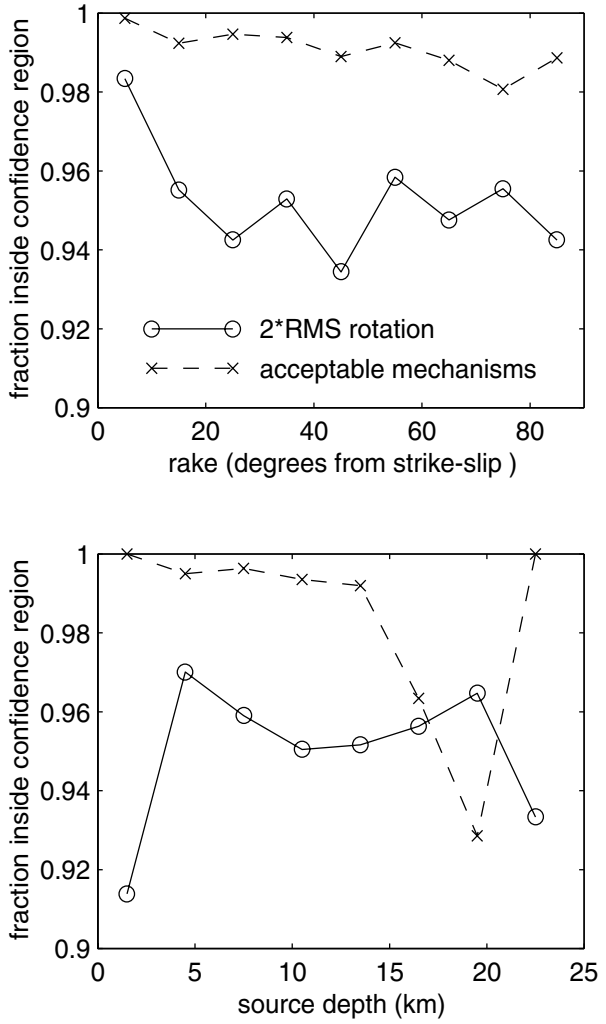

Figure 14. Two tests of the appropriateness of the uncertainty estimates for the same synthetic data as in Figure 13. Solid lines: The fraction of events for which the angular misfit between the preferred and correct solutions is less than the 2σ uncertainty, as estimated from the spread of the set of acceptable mechanisms. The correct solution should fall inside the 95% confidence region for approximately 95% of the events. Dashed lines: The fraction of synthetic tests for which the correct mechanism falls within the set of acceptable mechanisms. Ideally, it should always be included. Rake is defined to vary from 0° for pure strike-slip events to 90° for pure dip slip.

difficult to parameterize. This suggests that a nonparametric approach to uncertainty estimation should be taken. The instability of some focal mechanisms with respect to changes in location and velocity model also suggests that the assigned quality of a mechanism should be based not only on the number of misfit polarities but also on the stability of the solution. The focal-mechanism method introduced in this article incorporates both of these ideas.

These changes in methodology appear to have successfully improved the computed focal mechanisms. The improvement over the FPFIT technique is demonstrated using clusters of earthquake with very similar waveforms, which should therefore have very similar mechanisms. The well-constrained solutions found using our technique are very similar to each other, whereas those found by FPFIT contain a few very dissimilar mechanisms. Similar event clusters are quite valuable because they provide one of the few situations in which the correct focal mechanisms for small earthquakes are known. They also provide the only means for independently estimating the error rate of the polarity picks.

Another avenue toward improving focal mechanisms is to include other data besides *P*-wave polarities. The *S*-wave to *P*-wave amplitude ratio, which should vary systematically over the focal sphere, has previously been used to constrain focal mechanisms (e.g., Kisslinger *et al.*, 1981; DeNatale *et al.*, 1991; Rau *et al.*, 1996; Shen *et al.*, 1997). However, for the SCSN data we studied, the only systematic variation in *S*-to-*P* amplitude ratio is an inverse correlation with source–receiver distance. The high-frequency *S* waves recorded by the SCSN are presumably highly attenuated in the crust. The use of *S*-to-*P* amplitude ratios may be more practical with broadband data. *S*-wave polarities have also been used to constrain focal mechanisms (e.g., Nakamura and Yoshida, 2000). However, *S*-wave polarities may be controlled by shear-wave splitting if the crust is anisotropic, as was found in the Anza region of southern California (Aster *et al.*, 1990). Although we chose not to include either amplitude ratios or *S*-wave polarities in the examples in this article, they could readily be incorporated into the general methodology.

Conclusions

We have introduced a new method for constraining earthquake first-motion focal mechanisms, which differs from previous methods primarily in that it accounts for the possibility of errors in the computed takeoff angles. The set of acceptable focal mechanisms, allowing for the expected errors in polarities and takeoff angles, is found for each event. Because the sensitivity of focal mechanisms to changes in source location and seismic-velocity model is complex and poorly understood, we consider multiple combinations of reasonable source depths and 1D velocity models. All mechanisms with up to a given fraction of misfit polarities are included in the set of acceptable solutions. Mechanisms are considered adequately stable only if the set of acceptable solutions is tightly clustered. The mechanism uncertainty is represented nonparametrically as the set of acceptable mechanisms.

In tests on realistically noisy synthetic data, our method performs well. The correct mechanism falls within the set of acceptable solutions for ~99% of events, and the majority of the stable solutions are within 20° of the correct mechanism. Our method was also tested on a cluster of closely spaced events that have very similar waveforms. The well-constrained mechanisms for events in this cluster are very similar. Our method of uncertainty estimation successfully

filters out the ambiguous and unstable mechanisms. Mechanisms that are very dissimilar from the rest of the cluster, but that appear adequately constrained based on other quality criteria, are in fact unstable with respect to possible errors.

We also present a brief study of the sensitivity of first-motion focal mechanisms to changes in polarity observations, event depth, and seismic-velocity model. The mechanisms are most sensitive to the vertical velocity gradient and less so to the magnitude of the seismic velocity and the source depth. The mechanisms of dip-slip events are the most unstable with respect to errors, because changes in source location and velocity model affect the computed takeoff angles more than the ray azimuths. Shallow events are probably not as well constrained as deep events because of their greater sensitivity to location errors and because of the higher degree of heterogenity and hence, uncertainty, in the seismic-velocity structure of the shallow crust.

Acknowledgments

We thank Egill Hauksson for kindly allowing us to use his 3D seismic-velocity model and the ray azimuths and takeoff angles computed from it. We also thank Paul Reasenberg and David Oppenheimer for making their FPFIT software package available. Debi Kilb, Arthur Snoke, and an anonymous reviewer provided helpful comments that improved the manuscript. This work was supported by NEHRP/USGS Grant 01HQER0183. This research was supported by the Southern California Earthquake Center (SCEC). SCEC is funded by NSF Cooperative Agreement EAR-8920136 and USGS Cooperative Agreements 14-08-0001-A0899 and 1434-HQ-97AG01718. The SCEC contribution number for this paper is 647.

References

Aster, R., P. M. Shearer, and J. Berger (1990). Quantitative measurements of shear wave polarizations at the Anza seismic network, southern California; implications for shear wave splitting and earthquake prediction, *J. Geophys. Res.* **95,** 12,449–12,473.

DeNatale, G., A. Ferraro, and J. Virieux (1991). A probability method for local earthquake focal mechanisms, *Geophys. Res. Lett.* **18,** 613–616.

Hardebeck, J. L., and E. Hauksson (2001). The crustal stress field in southern California and its implications for fault mechanics, *J. Geophys. Res.* **106,** 21,859–21,882.

Hauksson, E. (2000). Crustal structure and seismicity distribution adjacent to the Pacific and North American plate boundary in southern California, *J. Geophys. Res.* **105,** 15,365–15,394.

Hauksson, E., and J. S. Haase (1997). Three-dimensional V_P and V_p/V_s velocity model of the Los Angeles Basin and central Transverse Ranges, California, *J. Geophys. Res.* **102,** 5423–5453.

Hauksson, E., L. M. Jones, and K. Hutton (1995). The 1994 Northridge earthquake sequence in California: seismological and tectonic aspects, *J. Geophys. Res.* **100,** 12,335–12,355.

Kilb, D. (2001). Fault parameter constraints using relocated earthquakes: implications for stress change calculations, *EOS* **82,** F811.

Kisslinger, C., J. R. Bowman, and K. Koch (1981). Procedures for computing focal mechanisms from local (*SV*/*P*) data, *Bull. Seism. Soc. Am.* **71,** 1719–1729.

Lund, B., and R. Slunga (1999). Stress tensor inversion using detailed microearthquake information and stability constraints: application to Olfus in southwest Iceland, *J. Geophys. Res.* **104,** 14,947–14,964.

McKenzie, D. P. (1969). The relation between fault plane solutions for earthquakes and the directions of the principal stresses, *Bull. Seism. Soc. Am.* **59,** 591–601.

Nakamura, M., and A. Yoshida (2000). Determination of focal mechanism solutions using initial motion polarity of P and S waves, *EOS* **81,** F870.

Rau, R.-J., F. T. Wu, and T.-C. Shin (1996). Regional network focal mechanism determination using 3D velocity model and *SH*/*P* amplitude ratio, *Bull. Seism. Soc. Am.* **86,** 1270–1283.

Reasenberg, P., and D. Oppenheimer (1985). FPFIT, FPPLOT, and FPPAGE: FORTRAN computer programs for calculating and displaying earthquake fault-plane solutions, *U.S. Geol. Surv. Open-File Rept. 85-739*, 109 Pp.

Richards-Dinger, K. B., and P. M. Shearer (2000). Earthquake locations in southern California obtained using source-specific station terms, *J. Geophys. Res.* **105,** 10,939–10,960.

Shearer, P. M. (1997). Improving local earthquake locations using the L1 norm and waveform cross-correlation: application to the Whittier Narrows, California, aftershock sequence, *J. Geophys. Res.* **102,** 8269–8283.

Shearer, P. M., J. L. Hardebeck, L. Astiz, and K. B. Richards-Dinger (2002). Analysis of similar event clusters in aftershocks of the 1994 Northridge, California, earthquake, *J. Geophys. Res.* (in press).

Shen, Y., D. W. Forsyth, J. Conder, and L. M. Dorman (1997). Investigation of microearthquake activity following an intraplane teleseismic swarm on the west flank of the Southern East Pacific Rise, *J. Geophys. Res.* **102,** 459–475.

Institute of Geophysics and Planetary Physics
Scripps Institution of Oceanography
University of California, San Diego
La Jolla, California 92093-0225
jeanne@igpp.ucsd.edu
(J.L.H., P.M.S.)

Manuscript received 20 July 2001.